Original Article

Detection of Pulmonary Nodules in Low-dose Computed Tomography Using Localized Active Contours and Shape Features

Zahra Nadealian, Behzad Nazari, Saeid Sadri, Mohammad Momeni[1]

Department of Electrical and Computer Engineering, Isfahan University of Technology, [1]Department of Radiology, Alzahra Hospital, Isfahan University of Medical Sciences, Isfahan 84156-83111, Iran

Abstract

Background: Pulmonary nodules are symptoms of lung cancer. The shape and size of these nodules are used to diagnose lung cancer in computed tomography (CT) images. In the early stages, nodules are very small, and radiologist has to refer to many CT images to diagnose the disease, causing operator mistakes. Image processing algorithms are used as an aid to detect and localize nodules. **Methods:** In this paper, a novel lung nodules detection scheme is proposed. First, in the preprocessing stage, our algorithm segments two lung lobes to increase processing speed and accuracy. Second, template-matching is applied to detect the suspicious nodule candidates, including both nodules and some blood vessels. Third, the suspicious nodule candidates are segmented by localized active contours. Finally, the false-positive errors produced by vessels are reduced using some two-/three-dimensional geometrical features in three steps. In these steps, the size, long and short diameters and sphericity are used to decrease the false-positive rate. **Results:** In the first step, some vessels that are parallel to CT cross-plane are identified. In the second step, oblique vessels are detected using shift of center of gravity in two successive slices. In step three, vessels vertical to CT cross-plane are identified. Using these steps, vessels are separated from nodules. Early Lung Cancer Action Project is used as a popular dataset in this work. **Conclusions:** Our algorithm achieved a sensitivity of 90.1% and a specificity of 92.8%, quite acceptable in comparison to other related works.

Keywords: *Computer-aided detection, computed tomography images, feature extraction, localized active contours, pulmonary nodules, template matching*

Introduction

Lung cancer in the early stages has no symptoms in serial computer tomography (CT) images, whereas its early detection can increase survival rate. The symptoms of lung cancer only appear in more serious stages due to characteristics and position of the nodules in the lungs.[1] Lung nodules are round- or egg-shaped lesions with regular or irregular boundaries. Nodules in early stages are very small, thus high-quality images need to be used, and these images need to be processed by a radiologist visually. In such a situation, computer-aided detection (CAD) systems process the CT images to assist the radiologist in detecting pulmonary nodules and increasing sensitivity and specificity. Suspicious areas are mainly due to blood vessels which resemble nodules.

In the remainder of this section, two categories of papers are investigated. The first category discusses nodule detection,[2-16] and the second group considers nodule segmentation.[17-23]

Murphy *et al*.[2] described a scheme for the automatic detection of nodules in thoracic CT scans that enhances false-positive reduction using two successive k-nearest neighbor classifiers. Liu *et al*.[3] proposed a computer-aided diagnosis system for lung nodule detection using the hidden conditional random field. This method achieved sensitivity of 89.3%. Keserci and Yoshida[4] proposed a new computer-aided diagnosis scheme for automated detection of lung nodules in digital chest radiographs based on combination of morphological features and wavelet snake model. Choi and Choi[5] presented an algorithm based on two-dimensional (2D) and three-dimensional (3D) features to reduce false-positive errors. This system first enhanced the CT images and then detected nodule candidates. Afterward, the features are extracted from every region of interest (ROI). The 3D geometric feature

How to cite this article: Nadealian Z, Nazari B, Sadri S, Momeni M. Detection of pulmonary nodules in low-dose computed tomography using localized active contours and shape features. J Med Sign Sens 2017;7:203-12.

Address for correspondence:
Ms. Zahra Nadealian, Department of Electrical and Computer Engineering, Isfahan University of Technology, Isfahan 84156-83111, Iran.
E-mail: z.nadealian@ec.iut.ac.ir

Website: www.jmss.mui.ac.ir

set consisted volume elongation factor, compactness, and approximated radius. In addition, the 2D features were extracted from middle slice of nodule candidates. These features were mean, variance, skewness, kurtosis, area, radius, and eight biggest eigenvalues. Finally, these features were applied as input to a genetic programming module. The method applied to 32 scans consisting of 153 nodules and 7528 slices. Half of dataset (16 scans) was used for training, and the remaining was used to test the classifier. This method achieved sensitivity of 92% with an average of 6.5 false-positives per scan. Suzuki *et al*.[6] investigated a pattern-recognition technique based on an artificial neural network for the reduction of false positives of detected lung nodules in low-dose CT.

Gao *et al*.[7] proposed a novel template-matching using Hessian matrix in a series of chest X-ray images. First, the lung lobes were extracted in the original images. Then, template-matching method was used to detect the suspicious nodule candidates. Although it was fast and nearly all nodules were detected, it had a high false-positive rate. Hence, to classify nodule candidates into two groups, nodules and vessel, a classifier based on eigenvalues of Hessian matrix was proposed. The algorithm depended on a few constants that had to be specified experimentally. This method was applied to both a high-resolution CT and to a normal CT. Yogananda *et al*.[8] proposed an algorithm to detect the pulmonary nodules. After preprocessing step, morphological operations were used to detect the nodule candidates. Then, to discriminate between the nodules and the vessels, the successive frames of the CT were examined. If the candidate was a vessel, the displacement of center of gravity of the candidate in successive frames was large. However, if the candidate was a nodule, the displacement would be small. This algorithm failed to separate the nodules from vertical vessels. Namin *et al*.[9] developed an automatic method for lung nodule detection. After preprocessing step, suspicious nodule candidates were detected on the basis of intensity and volumetric shape index (SI). This method achieved sensitivity of 88% with an average of 10.3 false positives per scan. Lin *et al*.[10] developed a neural network system based on a two-level convolution neural network architecture to reduce false positives. Shi *et al*.[11] employed neural network ensemble for false positives reduction in detecting lung nodules in chest radiographs. The performance of this algorithm was evaluated by use of FROC. Dolejsi *et al*.[12] designed a CAD system both to detect small pulmonary nodules efficiently and to reduce false positives based on Asymmetric Adaboost ensemble. Guo *et al*.[13] proposed a scheme on the basis of an adaptive classification system. Eight features were extracted from nodule candidates, and support vector machine (SVM) was used as a nonlinear classifier. Assefa *et al*.[14] proposed an algorithm using template-matching and multiresolution analysis to improve false-positive rate. In this algorithm, intensity and multiresolution features were used. This method achieved detection rate of 81.212% and false-positive rate of 35.15%. Farag *et al*.[15] determined the models for lung nodule detection by template-matching method. This algorithm emphasized on the features using texture and shape properties of nodules. de Carvalho Filho *et al*.[16] proposed an algorithm based on taxonomic diversity and taxonomic distinctness indexes from ecology to describe the texture of nodule and nonnodule candidates. Then, SVM was used as a classifier. This algorithm achieved a mean accuracy of 98.11%.

By considering the abovementioned papers, there are generally two approaches in nodule detection: detection using only a single 2D frame and detection using a series of 2D frames. As it is heuristically clear, experiments show that detection results are much better, when multiple frames are used for diagnosis. Furthermore, the experimental results have shown that accurate segmentation of regions in CT images has a significant effect in the diagnosis of pulmonary nodules. Therefore, many algorithms have been developed for this purpose.[17-23] In the following, a brief explanation of algorithms used for lung nodule segmentation is presented.

Messay *et al*.[18] used a regression neural network to determine threshold parameters in lung nodule segmentation. They tested their algorithm on 66 lung nodules and achieved a segmentation accuracy of 80%. Qian and Guirong[20] proposed the expectation maximization (EM) algorithm for lung nodule detection and segmentation. Their model was independent from the size of nodules. Sun *et al*.[21] developed an automatic segmentation algorithm of nodules in CT images. This method successfully distinguished nodules attached to pleural surface, but it failed to segment the cavity nodules. Zinoveva *et al*.[22] proposed a soft segmentation based on pixel-level texture features using a decision-tree classifier with classification and regression tree algorithm. This method successfully distinguished the nodules that were attached to vessels, but it failed to segment those attached to the chest wall. To solve this problem, the lung segmentation was performed in the preprocessing step. Okada and Akdemir[23] proposed a segmentation method using SI. This algorithm provided successful results to segment the spherical nodules, but it failed to detect the nonspherical nodules. The model used in this paper successfully segmented ground-glass opacity (GGO) nodules, cavity nodules, and nodules that are attached to vessels or chest wall.

To achieve a high-performance level for lung nodules detection, an efficient method employs three major steps: initial nodule detection, segmentation process, and false-positive reduction. In this study, we employed a template matching (TM) method to increase the detection sensitivity. Then, we utilized a local active contour to

increase segmentation accuracy; this method is able to segment challenging nodule candidates (vessels, different types of nodules including GGO nodules, cavity nodules, spherical and nonspherical nodules, and nodules that are attached to vessels or chest wall) that some previous works fail. Finally, we proposed a three step false-positive reduction algorithm; this approach was used to distinguish nodules from other suspicious regions including oblique blood vessels and vessels that are parallel or vertical to CT cross-plane. The main novelties of this work are automated nodule detection along with discriminating nodules from different type of vessels using shape features, which leads to a high sensitivity and specificity. Figure 1 gives an overall overview of our scheme for nodule detection in CT images. Accordingly, the remainder of this paper continues as follows: our proposed algorithm is presented in Section 2. In Section 3, we discuss the experimental results. Conclusion is given in Section 4.

Materials and Methods

Preprocessing process

Nodule detection process is divided into the following steps: preprocessing, identification of suspicious nodule candidates, classification, and false-positive reduction. In the preprocessing stage, the lung lobes are segmented in CT images. The approach proposed in[24] is used to segment the lung from its surrounding based on EM algorithm and morphological operations. Furthermore, contrast adjustment is applied to improve the quality of the lung lobe images. A sample is shown in Figure 2.

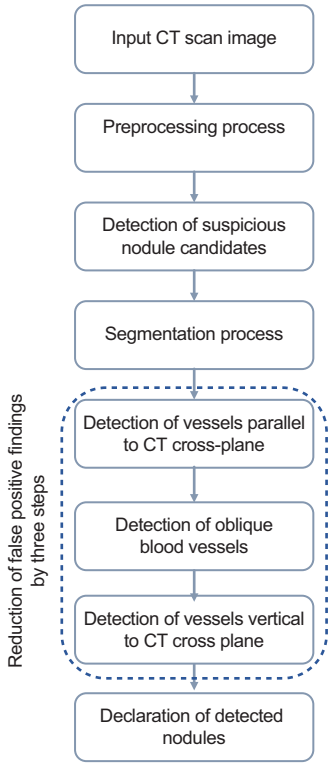

Figure 1: Flowchart for nodule detection procedure

Detection of suspicious nodule candidates

TM can be used to detect the pulmonary nodules efficiently, but at the same time many vessels are also detected as nodules in this manner.[7] Intensity value of nodules usually has a Gaussian-like distribution as follows:[15]

$$q(r) = q_{\max} * e^{-(r/\rho)^2},\ 0 \le r \le R \quad (1)$$

Where,

$$\rho = R\left(\ln\left(q_{\max}\right) - \ln\left(q_{\min}\right)\right)^{-0.5}$$

In which $q_{\min}$ and $q_{\max}$ are the minimum and maximum of nodule intensity, $q(r)$ is the intensity of nodule at distance from the centroid of the nodule, and R is the radius of nodular template.

TM method computes the normalized cross-correlation (NCC) of the image and the template by the following equation:

$$\gamma = \frac{\sum_{x,y}\left[f(x,y) - \overline{f_{u,v}}\right]\left[t(x-u,y-v) - \bar{t}\right]}{\sqrt{\sum_{x,y}\left[f(x,y) - \overline{f_{u,v}}\right]^2 \sum_{x,y}\left[t(x-u,y-v) - t\right]^2}} \quad (2)$$

Where

$$\overline{f_{u,v}} = \frac{1}{N_x N_y}\sum_{x=u}^{u+N_x-1}\sum_{y=v}^{v+N_y-1} f(x,y)$$

$f(x,y)$ and $\overline{f_{u,v}}$ are the input image and its mean value in the region under template located at (u,v), $t(x,y)$, is the nodule model and its mean value is $\bar{t}$. In (2), the correlation coefficient γ varies between 1 and −1. If the correlation coefficient is γ above a positive threshold level, the point (u,v) is accepted to belong a suspicious nodule candidate.[7] This threshold level according to our database is experimentally set to 0.6.

In our experiments, we used a library of circular and semi-circular templates with 90° rotations with a Gaussian distribution of grayscale intensity. The mean diameter of nodules in our database is 8.5 mm with a standard deviation of 3.6 mm. Accordingly, we chose a diameter of 8.5 mm for our circular and semi-circular templates the same as.[15]

Using this method, many regions are tagged, but the true positive rate is high. Figure 3 shows a sample of this method. The template image is seen as Figure 3a. After removed interference, the pulmonary parenchyma image is gotten by best weight segmentation and seen as Figure 3b. The normalized cross-correlation of the image and the template is seen as Figure 3c and the initial regions of interest are shown as Figure 3d.

It should be noted that in the above procedure, some vessels are also detected as suspicious nodule candidates.

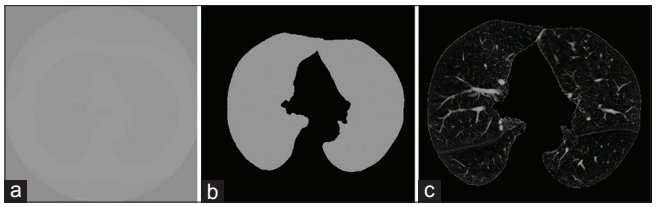

Figure 2: Lung lobe segmentation with contrast adjustment. (a) Input image, (b) mask of segmented lung region, (c) segmented lung

2D processing is frequently not able to remove the interference of vascular, leading to high false-positive rate. To separate the nodules from vessels in the next section, nodule candidates are segmented, and then these segmented nodule candidates are classified using some features.

Segmentation process

Accurate segmentation of suspicious nodule candidates, that could be a nodule or a vessel, is very important. Segmentation of nodule candidates is challenging because of the following three effects: noise, nodules that are attached to blood vessels or attached to lung wall, and low contrast of intensity values between nodules and other structures in CT images, due to low-dose CT imaging.

The basic idea in active contour models is to allow a contour to deform so as to minimize a given cost function to provide the desired segmentation results. In general, there are two main categories of active contour models: edge-based and region-based.

Edge-based active contour models mainly utilize the edge and gradient information to drive the contours to identify object boundaries. The result of image segmentation by these models is highly dependent on the initial contour placement and very sensitive to image noise.

Compared with edge-based active contours, region based active contours model the foreground and background regions statistically and optimize a global energy cost function. These models are less sensitive to initialization and image noise. Region-based active contours focus on a localized energy function based on piece-wise constant model of Chan and Vese (C-V model),[25] which can be written as:

$$F(u,v,\phi) = \mu\int_{\Omega}\left|\nabla H(\phi)\right| dx + \nu\int_{\Omega} H(\phi)\ \ dx$$
$$+\lambda_1\int_{\Omega} H(\phi)(I-u)^2\ \ dx + \lambda_2\int_{\Omega}(1-H(\phi))(I-v)^2\ \ dx \qquad (3)$$

Where I is a given image defined on domain Ω, υ, and are ν the global mean intensities of the interior and exterior regions. λ_1, λ_2, ν and μ are positive constant coefficients and is $H(\phi)$ Heaviside function.

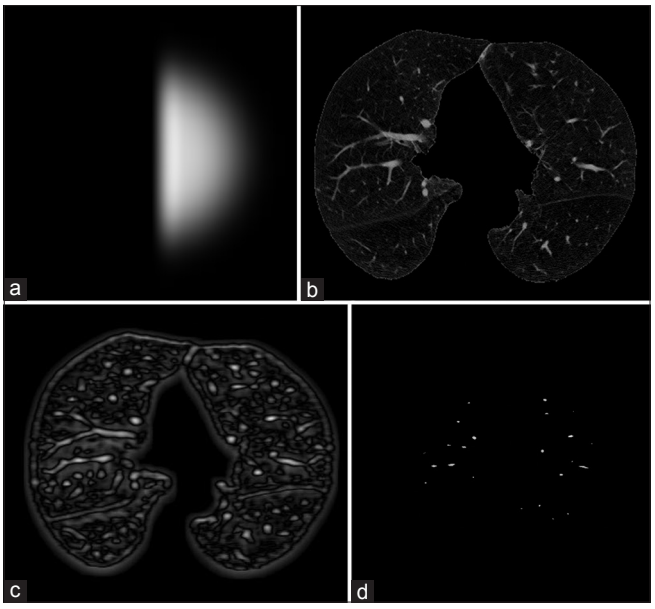

Figure 3: Suspicious nodule candidate detection. (a) Template, (b) original image, (c) normalized cross-correlation of image and template, (d) result of template matching method

Optimizing global statistics usually is not ideal for segmenting heterogeneous objects.[26] Therefore, to accurately segment these objects, a new model of active contour is developed which utilizes local information.

Localized active contours are capable of segmenting objects with heterogeneous feature profiles.[27] In this approach, segmentation is not based on global region models. The average intensities in interior and exterior areas of a mask $B(x,y)$ are computed at each point. To optimize the total energy of the contour, the mask is considered in each point separately, and the point is moved to decrease the energy function. This energy function is defined as following:

$$E(\phi) = \int_{\Omega_x}\delta\phi(x)\int_{\Omega_y} B(x,y).F(I(y),\phi(y))\ \ dxdy \qquad (4)$$
$$+\lambda\int_{\Omega_x}\delta\phi(x)\left\|\nabla\phi(x)\right\| dx$$

F is a generic internal energy, and $\delta\phi(x)$ is Dirac function. Using $B(x,y)$, F operates only on local image information in neighborhood of (x,y) and λ is a smoothing parameter. Using calculation of variation results:

$$\frac{\partial\varphi}{\partial t}(x) = \delta\phi(x)\int_{\Omega_y} B(x,y)\ \ \delta\phi(y).$$
$$\left(\left(I(y)-u_x\right)^2-\left(I(y)-v_x\right)^2\right)dy + \lambda\delta\phi(x)div\left(\frac{\nabla\phi(x)}{\left|\nabla\phi(x)\right|}\right) \qquad (5)$$

The localized equivalents of and that defined in terms of the $B(x,y)$ function, u_x and v_x:

$$u_x = \frac{\int_{\Omega_y} B(x,y).H\phi(y).\mathrm{I}(y)dy}{\int_{\Omega y} B(x,y).H\phi(y)dy} \qquad (6)$$

$$v_x = \frac{\int_{\Omega_y} B(x,y).(1-H\phi(y)).\mathrm{I}(y)dy}{\int_{\Omega_y} B(x,y).(1-H\phi(y))dy} \quad (7)$$

Local active contour has three parameters, maximum iterations which is set to 200, local radius ($B\ (x,y)$) set to 1 and smoothing parameter (λ) set to 0.2. The parameters are chosen according to nodule specifications experimentally.

Figure 4 compares the results of global and local active contours applied to segmentation of a nodule. It can be seen that local active contour successfully segmented the nodule candidates with concave and low contrast boundaries.

This model was tested on different kinds of nodule candidates including both nodules and vessels. The experiments show the robustness and reliability of the model. As shown in Figure 5, this method successfully segmented nodule candidate regions from adjacent structures in majority of cases but failed to discriminate between background and some vessels. Figure 6 shows a vessel segmented by localized active contour. As it is shown in this figure, some gaps are generated within vessels. It should be noted that such a failure makes no problem in the final results because vessels are identified from nodules and omitted in later stages.

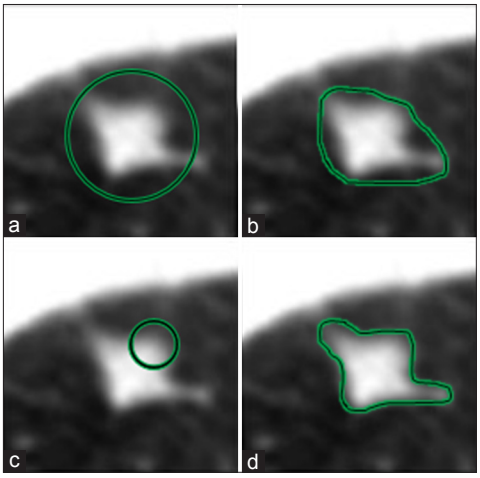

Figure 4: (a and c) Initialization, (b) final result with global energies, (d) final result with local energies

Discriminating blood vessels from nodules

In each CT cross-section, some vessels may resemble nodules, causing false nodule candidates which must be identified and omitted. The following three steps do the job. Nonnodule objects can be discriminated from nodule candidates using information of nodules such as size, volume, sphericity, and compactness.

Detection of vessels parallel to computed tomography cross-plane

Geometrical shapes of pulmonary nodules and vessels are spherical and cylindrical, respectively. A slice in a sphere, semi-sphere, vertical, or nearly vertical cylinder is circular or nearly circular. As the cylinder inclines more parallel to CT cross-plane, the difference between the long diameter and the short diameter increases. The long diameter is the distance between two points of nodule boundary with maximum distance, and the short diameter is the longest chord perpendicular to the long diameter.

We use long diameter/short diameter as a feature to classify vessels and nodules. The ratio is large for oblique vessels or vessels vertical to CT cross-plane and is small for nodules. The diagrams in Figure 7 show the distribution of long diameter/short diameter for nodules and vessels. The diagram vertical axis is the number of nodules/vessels with specific long diameter/short diameter of horizontal axis. The threshold value is experimentally set to 2.1. Some of the vessels that are detected or not detected in this step

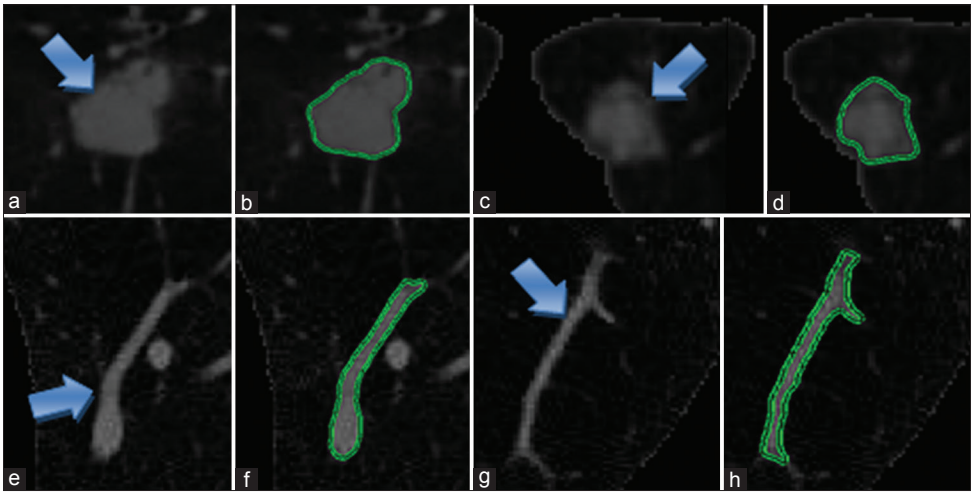

Figure 5: Segmentation results. (a and c) are nodule and (e and g) are vessel that are shown by blue arrows, (b, d, f and h) are the contour of the segmentation

are shown in Figure 8. In the next steps, remaining nodule candidates are examined to detect other possible vessels.

Detection of oblique blood vessels

If we consider the center of gravity of a nodule or vertical vessel in two successive slices, there would be a small displacement between these two centers [Figure 9], whereas this displacement would be greater for an oblique vessel. The diagrams in Figure 10 show the distributions of these displacements for nodules and vessels. Hence, a number of oblique blood vessels in nodule candidates can be identified using a threshold on these displacements. The diagram vertical axis is the number of nodules/vessels with specific displacements of horizontal axis. The threshold value is experimentally set to 0.75.

Detection of vessels vertical to computed tomography cross-plane

In the previous two steps, oblique and parallel vessels were removed from the suspicious nodule candidate list. In the current step, we will only consider the remaining suspicious nodule candidates. A vessel is not a compact object and continues to be connected in consecutive slices of CT images.[5] On the contrary, a nodule as shown in Figure 11 is a compact and sphere object, so its cross-section on a CT slice is nearly a semi-circle.

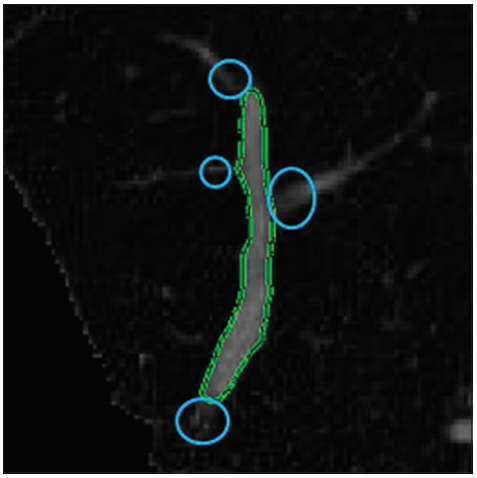

Figure 6: Parts of the vessel similar to background are shown inside blue circles and the contour of the segmentation is shown in green

Experimental results indicated that there is a small difference between the length and short diameter of a nodule, whereas the difference would be higher for vascular areas because vascular areas continues to be connected in successive slices of 2D CT images. Thus, the length and short diameter of remaining suspicious nodule candidates are extracted as features. Furthermore, the length of nodule candidates is calculated as follows:

$$\text{Length} = n \times \text{slice thickness} \quad (8)$$

n is the number of slices that transverses a nodule candidate. In this study, slice thickness of data is mm. To determine, the following algorithm is applied as in Figure 12:

1. Three slices, the current slice and slices before and after it are considered
2. The cross-section area of nodule is already segmented by local active contour
3. Its relative area in previous and next frames are marked, and the brightest pixels in these marked areas are determined and labeled by points P_1 and P_2, respectively
4. P_1 and P_2 are selected as the center of the initial local active contours
5. The radius of the active contours is 2.

The following cases may occur as shown in Figure 12b and c.

1. Each contour in previous/next slice has just one region. $M_{p1} \mid M_{p2}$ is the center of gravity in this region. If the following two conditions are fulfilled, the candidate area is considered to belong to the current nodule candidate
   a. The average intensity in this region be greater than a threshold
   b. The displacement of its center of gravity with respect to the center of gravity of the current slice, shown with vectors $d_{p1} \mid d_{p2}$ be smaller than a threshold
2. If the region segmented in the previous/next slice has multiple areas or has just one pixel, as in Figure 12c,

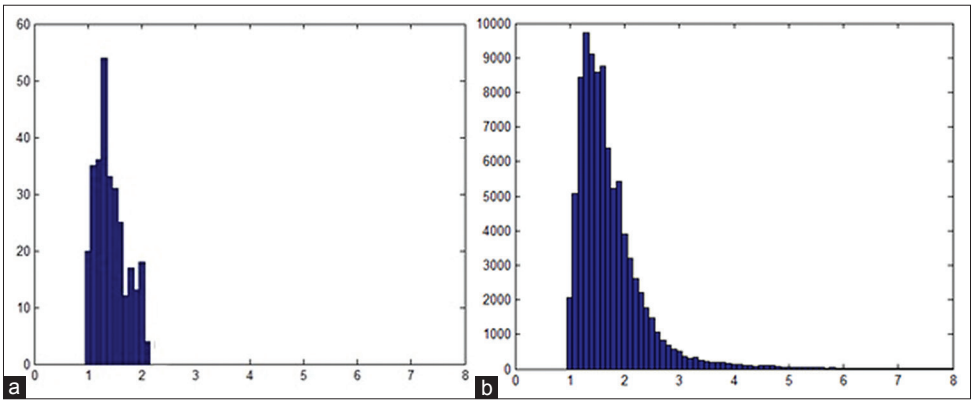

Figure 7: Histograms of long diameter/short diameter for (a) nodules, (b) vessels

the previous/next slice does not belong to the current nodule candidate.

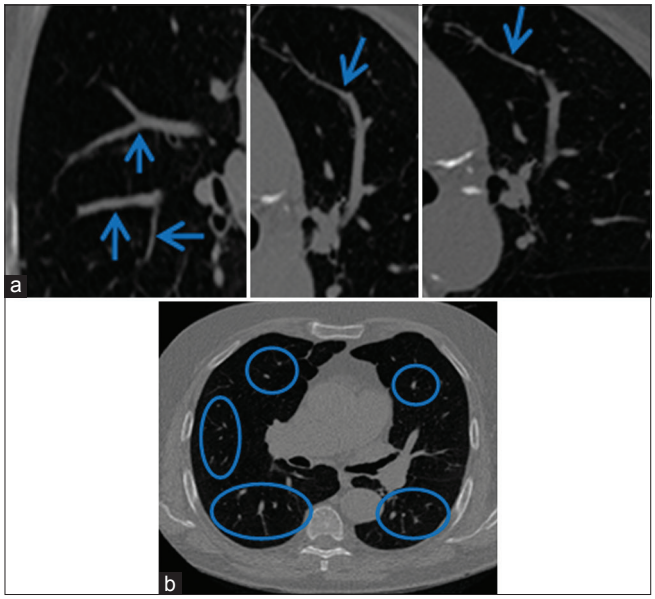

Figure 8: (a) Blue arrows show vessels detected in section 2.4.1, (b) Blue circles show vessels which resemble nodules but not detected in section 2.4.1

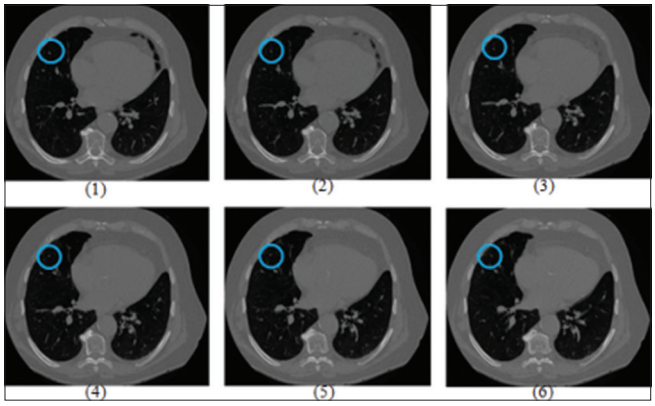

Figure 9: Vessel shown inside the blue circles in consecutive six computed tomography slices, vertical to computed tomography cross-plane

According to the above algorithm, the total number of slices belonging to the nodule *n* and so its length is determined.

The diagrams in Figure 13 show the scatter plot of the short-axis diameter and length for nodules and vessels. Using the features extracted from the regions, the length and short-axis diameter of the nodule candidates, SVM is used to classify the nodules and vessels. In experimental results, it is shown that SVM-RBF improves the performance of classification. This classifier is evaluated by 5-fold cross-validation.

Experimental Results

In this paper, we use the Early Lung Cancer Action Program public database, which is one of the lung image database consortium groups. This database contains fifty sets of low-dose CT lung scans taken at a single breath-hold with slice thickness 1.25 mm. The locations of nodules were certified by four radiologists. Accordingly, 31% of nodules are solitary, 30% are bronchiole attached, and 39% are lung wall attached, where 39.12% are juxtapleural nodules, 13.95% are vascularized nodules, 31.29% are well-circumscribed nodules, and 15.65% are pleural-tail nodules. The mean diameter of nodules in this database is 8.5 mm with standard deviation of 3.6.[28] It includes 50 sets of low-dose CT scans with a total of 12645 slices. CT scan images of 20 patients were used to develop the algorithm, and the remaining images were used to test the algorithm. The number of slices for a patient varies from 212 to 304. Slice thickness is 1.25 mm in this database, and pixel spacing is from 0.5078 mm to 0.8164 mm for different patients.

At first, we used TM method to find nodule candidates, and then we segmented the area of nodule candidates using localized active contours. Then most of the blood vessels were removed from the nodule candidate list according to the three steps in section 2.4. The parameters of all steps of the algorithm are chosen experimentally according to nodule specifications in CT images of our database.

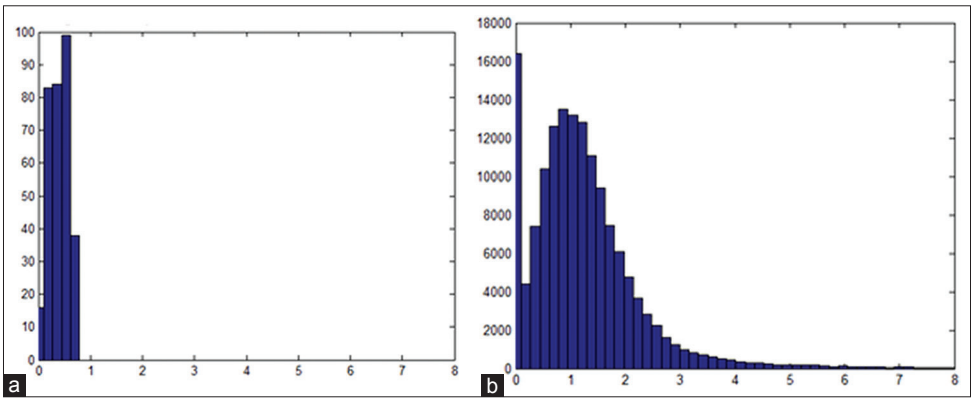

Figure 10: The histogram of the displacement between two centers for (a) nodules, (b) vessels

Sensitivity and specificity of our algorithm were 90.1% and 92.8%, respectively. Finally, the results were compared with some of the latest similar researches on the subject as shown in Table 1. In this table, the highest sensitivity is 96.15 in,[29] which is better than 90.1 of our algorithm, but our specificity is 92.8, better than 52.17 in.[29] This result shows that, compared with existing algorithms, our method performs at a similar or better level.

The receiver operating characteristic (ROC) curve is shown in Figure 14. ROC analysis was used to evaluate the automated classifier. The area under the ROC curve is a

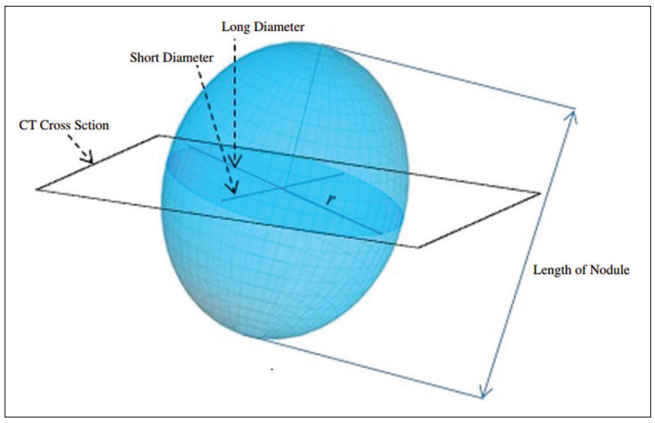

Figure 11: Feature parameters of a nodule

Table 1: Comparison between our method with relevant studies

Method	Sensitivity (%)	Specificity (%)	Database	Number of cases
Farag *et al*.[15]	85.22	86.28	ELCAP	50
Orozco *et al*.[29]	96.15	52.17	ELCAP and NBIA	75
Assefa *et al*.[14]	81.212	64.85	ELCAP	50
Our algorithm	90.1	92.8	ELCAP	30

NBIA – National biomedical imaging archives; ELCAP – Early Lung Cancer Action Project

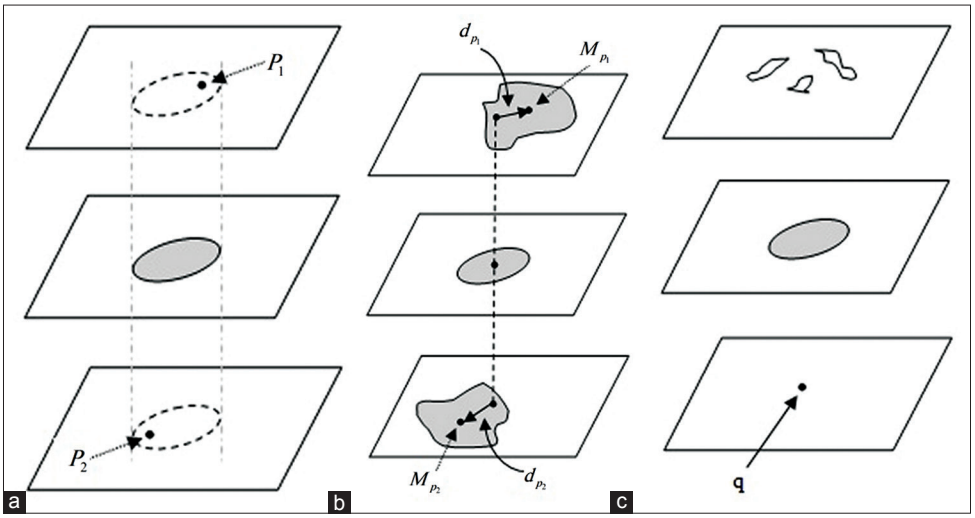

Figure 12: (a) Active contour of current slice and the two corresponding regions in previous and next slices. (b) Single regions segmented by local active contours in previous and next slices. (c) Multiple regions or one pixel

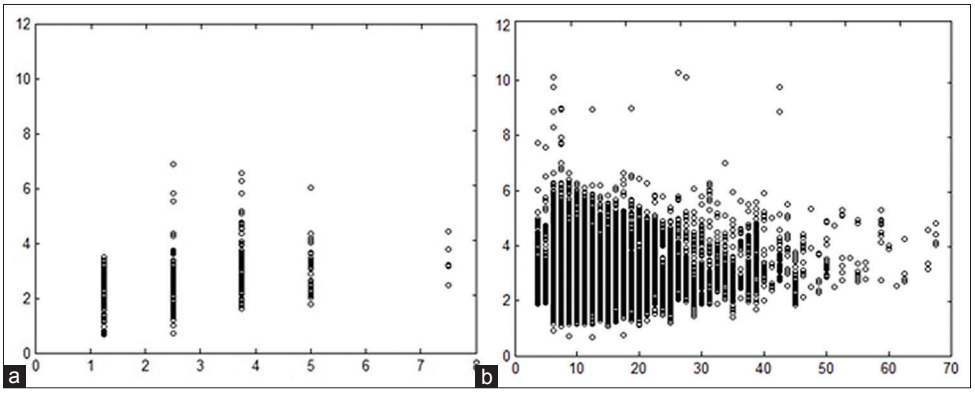

Figure 13: Scatter plot for short diameter versus length for (a) nodules, (b) vessels

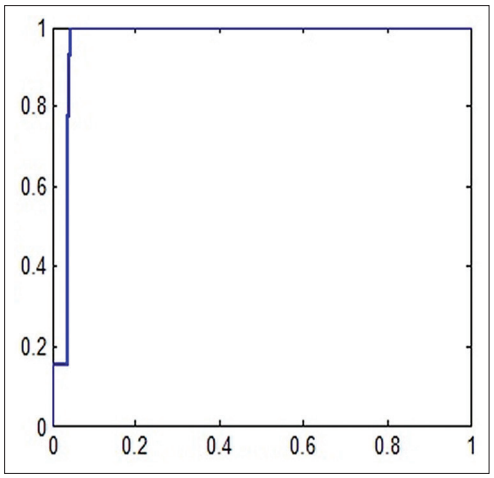

Figure 14: Receiver operating characteristic curve of proposed method

good measure of classifier performance. In this work, the area under the ROC curve was 0.94.

Our algorithm was run on a Core i5, 2.53 GHz CPU and 4G of RAM. The segmentation time of a suspicious nodule candidate was 5.0 s.

Conclusion

In this paper, a new algorithm for lung nodule detection was proposed. At first, TM method was used for detection of suspicious nodule candidates. Suspicious nodule candidates included both nodules and blood vessels. The nodule candidate regions were segmented, and then blood vessels were removed from the candidate list. This algorithm was evaluated on a dataset of fifty thoracic CT scans.

Our method is efficient for accurate detection of lung nodules in CT images. We compared the detection rate with previous existing methods; the proposed method performs similar or better. Localized active contour model provided superiority of our algorithm. Furthermore, our algorithm decreased false-positive rate using a three-step procedure using shape features.

Financial support and sponsorship

None.

Conflicts of interest

There are no conflicts of interest.

References

1. van Ginneken B, ter Haar Romeny BM, Viergever MA. Computer-aided diagnosis in chest radiography: A survey. IEEE Trans Med Imaging 2001;20:1228-41.
2. Murphy K, van Ginneken B, Schilham AM, de Hoop BJ, Gietema HA, Prokop M, *et al.* A large-scale evaluation of automatic pulmonary nodule detection in chest CT using local image features and k-nearest-neighbour classification. Med Image Anal 2009;13:757-70.
3. Liu Y, Wang Z, Guo M, Li P. Hidden Conditional Random Field for Lung Nodule Detection. In: 2014 IEEE International Conference on Image Processing (ICIP); 27 October, 2014. p. 3518-21.
4. Keserci B, Yoshida H. Computerized detection of pulmonary nodules in chest radiographs based on morphological features and wavelet snake model. Med Image Anal 2002;6:431-47.
5. Choi WJ, Choi TS. Computer-Aided Detection of Pulmonary Nodules using Genetic Programming. In: Image Processing (ICIP), 2010 17th IEEE International Conference on 26 September, 2010. p. 4353-6.
6. Suzuki K, Armato SG 3rd, Li F, Sone S, Doi K. Massive training artificial neural network (MTANN) for reduction of false positives in computerized detection of lung nodules in low-dose computed tomography. Med Phys 2003;30:1602-17.
7. Gao Y, Lv Q, Feng Q, Chen WF. A New Method for Detection of Pulmonary Nodules. In: Bioinformatics and Biomedical Engineering, 2007: ICBBE; 2007. The 1st International Conference on 6 July, 2007. p. 980-3.
8. Yogananda BS, Mohana HS, Shivakumar G. Computer Aided Diagnosis for the Detection of Lung Nodules. IOSR J Eng 2012;2:134-6.
9. Namin ST, Moghaddam HA, Jafari R, Esmaeil-Zadeh M, Gity M. Automated Detection and Classification of Pulmonary Nodules in 3D Thoracic CT Images. In: Systems Man and Cybernetics (SMC), 2010 IEEE International Conference on 10 October, 2010. p. 3774-9.
10. Lin JS, Lo SB, Hasegawa A, Freedman MT, Mun SK. Reduction of false positives in lung nodule detection using a two-level neural classification. IEEE Trans Med Imaging 1996;15:206-17.
11. Shi Z, Suzuki K, He L. Reducing Fps in Nodule Detection using Neural Networks Ensemble. In: Information Science and Engineering (ISISE), 2009 Second International Symposium on 26 December, 2009. p. 331-3.
12. Dolejsi M, Kybic J, Tuma S, Polovinc KM. Reducing False Positive Responses in Lung Nodule Detector System by Asymmetric Adaboost. In: Biomedical Imaging: From Nano to Macro, 2008. ISBI 2008. 5th IEEE International Symposium on 14 May, 2008. p. 656-9.
13. Guo W, Wei Y, Zhou H, Xue D. An Adaptive Lung Nodule Detection Algorithm. In: Control and Decision Conference, 2009. CCDC'09. Chinese 17 June, 2009. p. 2361-5.
14. Assefa M, Faye I, Malik AS, Shoaib M. Lung Nodule Detection using Multi-Resolution Analysis. In: Complex Medical Engineering (CME), 2013 ICME International Conference on 25 May, 2013. p. 457-61.
15. Farag AA, Graham J, Elshazly S, Farag A. Data-Driven Lung Nodule Models for Robust Nodule Detection in Chest CT. In: Pattern Recognition (ICPR), 2010 20th International Conference on 23 August, 2010. p. 2588-91.
16. de Carvalho Filho AO, Silva AC, de Paiva AC, Nunes RA, Gattass M. Lung-nodule classification based on computed tomography using taxonomic diversity indexes and an SVM. J Signal Process Syst 2017;87:1-8.
17. Kubota T, Jerebko AK, Dewan M, Salganicoff M, Krishnan A. Segmentation of pulmonary nodules of various densities with morphological approaches and convexity models. Med Image Anal 2011;15:133-54.
18. Messay T, Hardie RC, Tuinstra TR. Segmentation of pulmonary nodules in computed tomography using a regression neural network approach and its application to the lung image database consortium and image database resource initiative dataset. Med Image Anal 2015;22:48-62.

19. Rudyanto RD, Kerkstra S, van Rikxoort EM, Fetita C, Brillet PY, Lefevre C, *et al*. Comparing algorithms for automated vessel segmentation in computed tomography scans of the lung: The VESSEL12 study. Med Image Anal 2014;18:1217-32.
20. Qian Y, Guirong W. Lung Nodule Segmentation using EM Algorithm. Vol. 1. In: Intelligent Human-Machine Systems and Cybernetics (IHMSC), 2014 Sixth International Conference on 26 August, 2014. p. 20-3.
21. Sun SS, Li H, Hou XR, Kang Y, Zhao H. Automatic Segmentation of Pulmonary Nodules in CT Images. In: Bioinformatics and Biomedical Engineering, 2007. ICBBE 2007. The 1st International Conference on 6 July, 2007. p. 790-3.
22. Zinoveva O, Zinovev D, Siena SA, Raicu DS, Furst J, Armato SG. A Texture-Based Probabilistic Approach for Lung Nodule Segmentation. In: International Conference Image Analysis and Recognition 22 June, 2011. Berlin, Heidelberg: Springer; 2011. p. 21-30.
23. Okada K, Akdemir U. Blob Segmentation using Joint Space-Intensity Likelihood Ratio Test: Application to 3D Tumor Segmentation. In: Computer Vision and Pattern Recognition, CVPR 2005, IEEE Computer Society Conference on 20 June, 2005. p. 437-44.
24. Farag A, Graham J, Farag A. Robust Segmentation of Lung Tissue in Chest CT Scanning. In: Image Processing (ICIP), 2010 17th IEEE International Conference on 26 September, 2010. p. 2249-52.
25. Chan TF, Vese LA. Active contours without edges. IEEE Trans Image Process 2001;10:266-77.
26. Kass M, Witkin A, Terzopoulos D. Snakes: Active contour models. Int J Comput Vis 1988;1:321-31.
27. Lankton S, Tannenbaum A. Localizing region-based active contours. IEEE Trans Image Process 2008;17:2029-39.
28. ELCAP Public Lung Image Database. Available from: http://www.via.cornell.edu/lungdb.html. [Last accessed on 2017 Sep 06].
29. Orozco HM, Villegas OO, Maynez LO, Snchez VG, Domnguez HD. Lung Nodule Classification in Frequency Domain using Support Vector Machines. In: Information Science, Signal Processing and Their Applications (ISSPA), 2012 11th International Conference on 02 July, 2012. p. 870-5.